Addressing metal centres in supramolecular assemblies

Mario Ruben,*[a] Jean-Marie Lehn[b] and Paul Müller[c]

Received 10th August 2006
First published as an Advance Article on the web 11th September 2006
DOI: 10.1039/b517267p

Supramolecular metal ion assemblies are deposited from their solutions onto highly orientated pyrolytic graphite (HOPG) substrates to be imaged by scanning tunnelling microscopy (STM). Since the structural and electronic information of STM measurements are strongly entangled, the spectroscopic interpretation and analysis of the images of such molecular assemblies has proven to be challenging. This *tutorial review* focuses on a general room temperature scanning tunnelling spectroscopy (STS) protocol, current induced tunnelling spectroscopy (CITS), applied to free-standing 1D and 2D arrangements of supramolecular metal ion assemblies rendering local tunnelling probabilities with submolecular resolution. The size of the investigated molecular assemblies was confirmed by comparison with X-ray crystallographic data, while the consistency of the spectroscopic investigations and of the determined positions of the metal ions within the assemblies was checked by DFT calculations. Due to the genuine level structure of coordinated metal centers, it was possible to map exclusively the position of the coordination bonds in supramolecular transition metal assemblies with submolecular spatial resolution using the CITS technique. CITS might thus constitute an important tool to achieve directed bottom-up construction and controlled manipulation of fully electronically functional, two-dimensional molecular designs.

1. Introduction

In the last decade the understanding of the electronic transport properties of molecular assemblies and of the physical properties of isolated molecular systems has made enormous steps forward revealing intriguing new physics. Thereby, the investigation of functional molecules on solid substrates is increasingly becoming an important aspect of nanoscience. In particular, molecular and supramolecular electronics and spintronics, understood as the integration of molecular structures to provide specific electronic functionality, is emerging as a competitive alternative to conventional top-down approaches for reducing both the feature size and the cost per functional unit. Towards this goal, a thorough understanding of the electronic behaviour of supramolecular assemblies in reduced dimensions and its abstraction into theoretical models is mandatory for designing complex circuits by a molecular bottom-up approach.[1]

By analogy with semiconductor quantum dots, a metal ion coordinated by supramolecular bonds can be considered as a

[a]*Institute of Nanotechnology, PF 3640, D-76021 Karlsruhe, Germany. E-mail: Mario.Ruben@int.fzk.de*
[b]*ISIS, Université Louis Pasteur, 8, Allée Gaspard Monge, BP 70028, 67083 Strasbourg cedex, France*
[c]*Physikalisches Institut III, Universität Erlangen-Nürnberg, Erwin-Rommel-Str. 1, 91058 Erlangen, Germany*

Mario Ruben

Mario Ruben studied Chemistry in Germany and Spain. He obtained his PhD in 1998 at the University of Jena, Germany. After a post-doctoral fellowship at the ISIS-ULP in Strasbourg, France, he moved in 2001 to the Institute of Nanotechnology, Karlsruhe. His research interests involve the design, synthesis and physical characterization of functional molecule-based systems and their implementation into operational nanosystems. He is the co-ordinator of several European networks (FUN-SMARTs I and II; BIOMACH, MULTIFUN) dealing with molecular nanodevices.

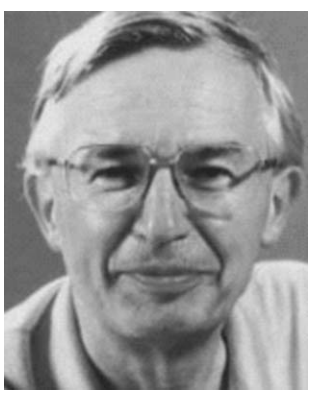

Jean-Marie Lehn

Jean-Marie Lehn was born in Rosheim, France in 1939. In 1970 he became Professor of Chemistry at the Université Louis Pasteur in Strasbourg and since 1979 has been Professor at the Collège de France in Paris. He received the Nobel Prize in Chemistry in 1987 for his studies on the chemical basis of "molecular recognition". Over the years his work led to the definition of a new field of chemistry, which he called "supramolecular chemistry". Author of more than 700 scientific publications, he is a member of many academies and institutions as well as of several industrial bodies. He has received numerous international honours and awards.

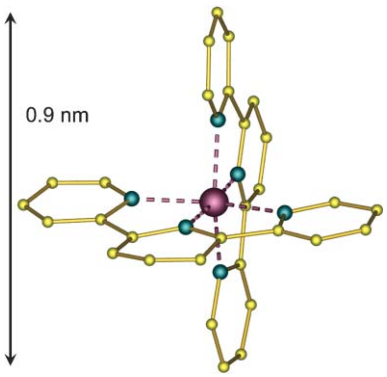

Fig. 1 $[Ni\text{-}(terpyridine)_2]^{2+}$ as a prototype of a mononuclear supramolecular coordination compound with the central metal ion acting as an ''ion-dot''.

natural quantum dot, *i.e.* the artificial atom is replaced by a real one. Typically the size of a single quantum dot is at least around 10 nm; however ''ion dots'', defined as isolated metal ion centres surrounded by their ligands, are more than one order of magnitude smaller in size (Fig. 1).[2a] Whereas the electronic level structure of a semiconductor quantum dot is controlled merely by its geometry, the levels of a coordinated metal ion are tailored by the type and geometrical arrangement of its ligands. The local distribution of electron density around the respective metal ion can be used as structural and functional base for the design of molecular devices. Consequently, the genuine redox-, electronic or spin states of metal ions and their explicit variability can be used to set the base of a novel kind of multistate digital information storage and processing. Local addressing of metal ions within supramolecular assemblies represents the first step towards the exploitation of the intrinsic physical properties of coordinated metal ions.

Supramolecular chemistry with its characteristic control of the self-assembly process and its intrinsic defect tolerance, has been proven to be a very efficient synthetic tool to achieve ordered arrangements of metal ions with sub-nanometer precision.[2] Recent progress in supramolecular coordination chemistry gives access to a broad variety of transition metal assemblies comprising organic ligands and metal ions of different nature with different redox and spin states and versatile functionalities (*e.g.* electronic, magnetic or optical).[3] In the following, square- (Section 3) and star-like (Section 4) arrays, and a supramolecular assembly embedded into a polyoxotungstate wheel (Section 6) will be discussed. Additionally to the discrete surpamolecular assemblies, the same experiments were also applied to an infinitely elongated metal ion assembly, a coordination polymer, in Section 5.

The exploitation of the physical properties at the single-molecule or, in particular, at the single metal ion level implicates the investigation of metal ion assemblies under restricted spatial dimensions. Several reports dealing with metal ion assemblies in nano-junctions (*e.g.* break junctions, electro-migration set-ups) have revealed an intriguing new insight into the electronic properties of such assemblies.[4]

However, this approach suffers from the drawback of restricted access to local structural information, which might be rather important, since the assembly–surface interaction seems to be of determining character for the understanding of the overall device behaviour. In view of its excellent real space imaging and manipulation capabilities, scanning tunneling microscopy (STM) is the method of choice to study supramolecular entities under restricted spatial dimensions, in particular on surfaces. It has recently been shown that supramolecular self-assembly and coordination processes can be steered on surfaces in a rational fashion.[5]

On the other hand, the structural and the electronic information of STM experiments are strongly entwined and the interpretation and analysis of rather complex supramolecular entities is not straightforward. In general, scanning tunneling spectroscopy (STS) can provide direct information about molecular energy levels, but such experiments require rigorous conditions (*e.g.* metal single crystals, ultrahigh vacuum, and low temperatures) to minimize environmental noise. The handling of often high-mass supramolecular assemblies under such drastic conditions has been shown to be rather difficult, as the classic ultrahigh vacuum deposition techniques like evaporation or sublimation would severely damage the molecules. Alternative spectroscopic techniques working under smoother conditions (*e.g.* room temperature, ambient pressure, solution deposition) would be of great advantage. The investigation of two-dimensional (2D) supramolecular nanoassemblies by STM on graphite surfaces was recently reviewed within this context.[6] It was shown, that under certain conditions room temperature experiments can also provide spectroscopic information about local changes of the electronic properties of molecular assemblies, *e.g.* resulting from intermolecular acceptor–donor,[7a] intermolecular π–π,[7b] and charge-transfer interactions.[7c]

2. Scanning tunneling microscopy and spectroscopy

Although scanning tunneling microscopy is capable of atomic resolution when imaging solid surfaces, mapping of large molecular assemblies with submolecular resolution is still challenging, in particular at ambient conditions. Merely mapping the van der Waals surface of often very dense molecular assemblies would only provide a featureless ''blob''

Paul Müller

Paul Müller was born in Forchheim, Germany in 1948. In 1988 he became member of staff of the Walther Meissner-Institute for low-temperature research of the Bavarian Academy of Sciences in Garching, Germany. He received the 1994 Walter Schottky prize for solid state research. Since 1995 he has been Professor for experimental physics at the University of Erlangen, Germany. He has authored more than 250 scientific papers. His current field of interest includes superconductivity, quantum computing, molecular electronics, scanning-probe microscopy, and biosensors.

of a large cluster of atoms. However, since STM images contain concomitantly both geometric and electronic information about the sample,[8] scanning tunneling spectroscopy (STS) can be used to probe electronic states of the entities investigated as a function of energy within the range of a few eV around the Fermi level.[9] If the investigated supramolecular objects possess energy levels within this energy range, which are at the same time well separated from other states of the molecule, STS should allow filtering them out energetically and to relate them to subunits of the molecular assembly. In this sense, both scanning tunneling microscopy (STM) and scanning tunneling spectroscopy (STS) techniques were applied to supramolecular assemblies arranged into either one-dimensional chains or two-dimensional layers or groups of free–standing single molecules.

In order to study the electronic properties of the supramolecular assemblies on surfaces, the current imaging tunneling spectroscopy (CITS) protocol was applied. In CITS, both topography and current–voltage characteristics (*I–V*) data of a surface-deposited object are recorded simultaneously.[9] At any pixel of the normal STM topography image being recorded with constant tunneling current *I*, the current control is released for a short time and *I–V* characteristics are measured. This results in an additional three-dimensional data set $I(V, x, y)$, whereby *x* and *y* are the spatial positions on the surface. The data can be displayed as a series of current images (CITS maps) representing the tunneling current *I* as a function of the lateral *x, y* coordinates at a given voltage *V* (see Fig. 2d, 3d, 6d, for example). At certain bias voltages, the contrast of these images changes significantly when new molecular energy levels come into play. The use of current imaging allows energy-resolved spectroscopy to be performed with spatial resolution, *i.e.* the density of states of the molecule can be visualized as a function of energy and position.[10] Alternatively, a series of *I–V* characteristics can be displayed along any trajectory across the image area. This allows the energy landscape of the molecule across any path of the image to be traced (see Fig. 5 and 9, for example).

Although this technique has been applied successfully to semiconductor materials, its application to organic molecules is rather difficult because of their mobility or instability.[11] Nevertheless, if there are energy regions where the molecular levels exclusively result from some functional subgroups of atoms, a selective screening of parts of the molecule would be possible, provided that the tip of the microscope could be placed in a stable way above them.

Such a situation might occur for a transition metal center embedded into a set of organic ligands *via* coordination bonds. The bonding situation within the molecular assembly provides a pronounced d-orbital character to the highest occupied states (HOMOs) and the lowest unoccupied states (LUMOs). Indeed, our DFT calculations show clearly that this is the case for all of our investigated supramolecular assemblies (*vide infra*). In fact, in the energy range of ± 1.5 eV related to the position of the Fermi-level E_F, which is accessible to tunneling spectroscopy at ambient conditions, several maxima of the density of states are present. This type of spectroscopy is exemplified in Fig. 2: Here, a monomer of a coordination polymer consisting of a Cu ion coordinated by an organic ligand (see Section 5) is scanned along the yellow line in Fig. 2a.

The molecule is deposited onto a (semiconducting) HOPG substrate. In general, for a STM measurement, there would be tunneling barriers between molecule and substrate and between molecule and STM tip (Fig. 2b). As the potential difference *U* is applied between tip and substrate, the position of the molecular energy levels is not fixed relative to the Fermi levels E_F of either substrate or STM tip (see discussion of Section 6). However, in most cases, due to a weak charge exchange between molecule and HOPG substrate, the tunneling barrier between substrate and molecule can be neglected and the molecular energy levels are fixed relative to the Fermi energy of the substrate. A negative potential of the substrate

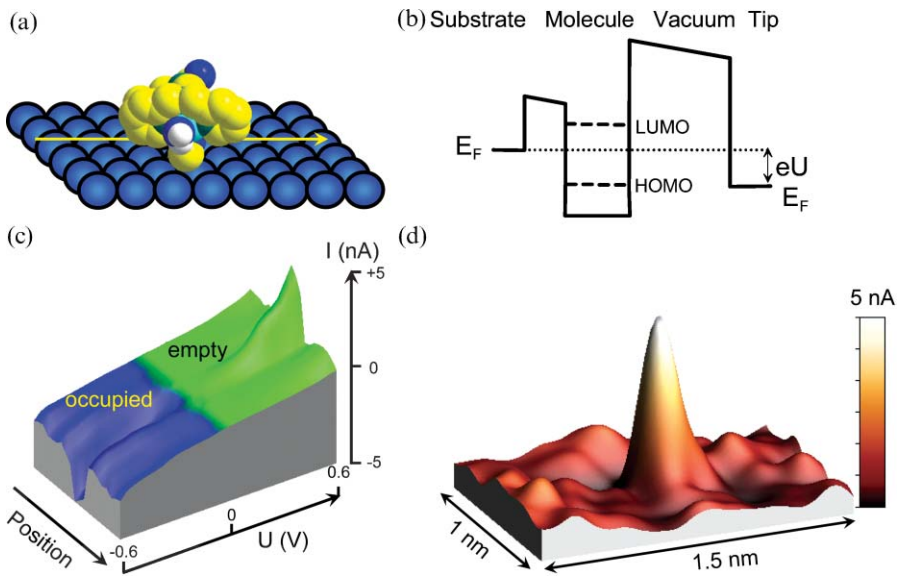

Fig. 2 a) Sketch of a molecule with a metal center deposited onto a HOPG substrate (blue spheres). b) Energy landscape for tunneling from a molecule deposited onto a substrate. c) Set of *I–V* curves measured along the yellow scan line in a. d) 3D current map taken at a bias voltage of 0.6 V.

with respect to the tip (Fig. 2b) allows the Fermi level of the tip to be scanned along the occupied molecular levels, whereas positive bias voltages probe the vacant levels (see Fig. 2c).

I–V characteristics are measured at any pixel of the scan. Subsequently, a 3D plot is generated from these spatially resolved *I–V*'s as displayed in Fig. 2c. At the position of the metal ion, certain bias levels conform to a resonant condition with either occupied (HOMO) or vacant (LUMO) molecular orbitals (see Fig. 2b). As a consequence, the tunneling current increases drastically and kinks in the *I–V* characteristics occur. Therefore, the resulting current map taken at bias values exceeding these levels will exhibit a distinct maximum at the position of the metal ion. This procedure can be applied for any scan line of the picture thus generating a huge data set which can be evaluated in several ways as described above. As an example, a current map for a set of scan lines covering an area of 1.0×1.5 nm^2 around the position of the molecule is shown in Fig. 2d. Here, the measured tunneling current is plotted *vs*. position for a bias level of +0.6 V. Maps with different bias levels can be generated from the data set as well. We emphasize that, in principle, this type of map can be measured directly by scanning with the corresponding bias level. However, scanning at high bias levels with current settings of several nA can cause the tip to crash into the molecule rather easily and is impracticable at least under ambient conditions.

Experimentally, a homemade scanning tunneling microscope exhibiting extremely reduced drift was used in the experiments to keep the STM tip stable above the object of investigation.[12] This microscope was equipped with a commercially available low-current control system (RHK Technology). The investigated supramolecular assemblies were always deposited onto highly orientated pyrolytic graphite (HOPG). The samples could be conveniently prepared by slow evaporation of aqueous acetonitrile solutions (typically between 10^{-8} and 10^{-10} M) of the respective supramolecular assemblies under ambient conditions. Before adding the solution onto the substrate surface, the resolution of the tunneling tip was calibrated against the distances of the known atomic spacing of the HOPG. In the experiments, tunneling currents between 5 and 200 pA and bias voltages between ± 50 and ± 500 mV were employed. For topography the scan frequency was varied between 2 and 5 Hz with a resolution of 256×256 points. For the CITS measurements, the scan frequency was reduced to approximately 0.3 Hz with a resolution of 128×128 points. Thereby, the CITS studies were performed by the interrupted-feedback-loop technique. This was carried out by opening the feedback loop to fix the separation between the tip and sample and ramping of the bias voltage over the range of interest. The scan range of voltages was typically from -1.0 V to 0.1 V relative to the tip potential for approximately 100–140 discrete voltage steps. Typically, tunneling resistances of the order of 5 GΩ were set. Pt–Ir (90/10) tips mechanically cut from wires with a diameter of 0.25 mm were used in all investigations reported below.

A useful insight into the origin of the maxima present in the CITS maps was provided by first-principle calculations of the electronic structure. These calculations have been carried out in the framework of density functional theory (DFT). The supramolecular metal ion assemblies described here were calculated using two different DFT approaches: (i) For the $[2 \times 2]$ grid-like metal ion assembly (**1**) ($[Co^{II}_4\mathbf{L^1}_4](BF_4)_8$, $\mathbf{L^1}$ = 4,6-bis(2′,2″-bipyrid-6′-yl)-2-phenyl-pyrimidine), the Naval Research Laboratory Molecular Orbital Library (NRLMOL) program package was used, which is an all-electron implementation of DFT. NRLMOL combines large Gaussian orbital basis sets, numerically precise variational integration and an analytic solution of Poisson's equation in order to accurately determine the self-consistent potentials, secular matrix, total energies, and Hellmann–Feynman–Pulay forces.[13] (ii) Assemblies (**3**) ($\{Fe^{III}[Fe^{III}(\mathbf{L^3})_2]_3\}$, $H_2\mathbf{L^3}$ = *N*-methyldiethanolamine) and (**5**) ($[Cu_{20}Cl(OH)_{24}(H_2O)_{12}(P_8W_{48}O_{184})]^{25-}$) were calculated using the computer code Siesta with strictly confined numerical atom-centered basis functions.[14] A recent review dealing with DFT calculations on molecules of comparable nature to those described here can be found in reference 15. The DFT calculations presented herein do not include possible interactions between molecule and substrate, which may account to some extent for the discrepancies between theory and experiment.

3. Grid-type supramolecular transition metal assemblies

Supramolecular transition metal assemblies of grid-type architecture comprise two-dimensionally ordered arrays of metal ions interconnected by sets of organic ligands. This class of compound is of particular interest as a structural platform for information storage devices, logic, and electrical switches.[3] The intrinsically regular network-like positioning of the metal ions within the grid-like molecules resembles strongly the binary coded matrix and crossbar architectures used in conventional information storage and processing technology. Furthermore, the redox,[16] magnetic,[17] and spin state[18] features of such complexes have been thoroughly investigated and are attractive for switching processes. In analogy to arrays of the much larger semiconductor quantum dots, grid-like assemblies might display ''ion-dot'' type features, if addressing could be realized within a scale of 1nm, that means to being able to realize ''read'' and ''write'' processes at the single metal-ion level. Due to their genuine geometry, flat deposition of grid-like complexes onto solid surfaces delivers automatically large domains of highly ordered metal ions within a grid-of-grids type arrangement.[19]

A number of square $[n \times n]$ grid-like assemblies with $n \leqslant 4$ has been obtained for transition metal ions with mainly octahedral coordination geometry. Among the assemblies defined by $n = 2$, the $[2 \times 2]$ Co^{II}_4 complexes have shown remarkable electronic[16] and optical properties (Fig. 3a).[20] In order to exploit these properties at the submolecular level, a drop of a solution of molecules of complex $[Co^{II}_4\mathbf{L^1}_4](BF_4)_8$ (**1**) ($\mathbf{L^1}$ = 4,6-bis(2′,2″-bipyrid-6′-yl)-2-phenyl-pyrimidine) in acetonitrile (10^{-9} M) was deposited on a HOPG substrate. Different molecular arrangements of $[2 \times 2]$ Co^{II}_4 grid-like assemblies could be observed after repeated scanning: 2D arrays, 1D lines (Fig. 3b) and isolated, free standing units of (**1**) (Fig. 3c). At very low coverage, a well ordered distribution of isolated entities could be observed. This demonstrates the

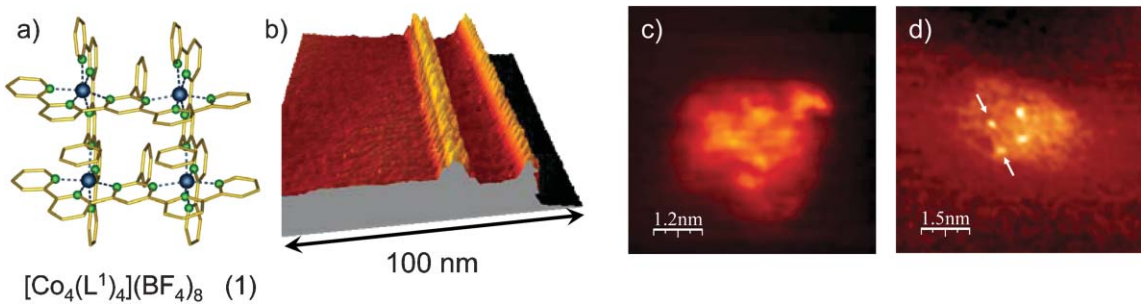

Fig. 3 [2 × 2] grid-like complexes: a) molecular structure of $[Co^{II}_4(\mathbf{L^1})_4](BF_4)_8$ (**1**); b) 3D representation of a STM topography image of a line of [2 × 2] grid complexes attached to monocrystalline steps of HPOG; c) experimental topography map of a single complex; d) experimental CITS map at −0.942 V.

delicate adsorbate–substrate interactions in this system, since thermal mobility becomes appreciable at room temperature.[21] Fig. 3b shows how molecules of (**1**) can be ordered along the monocrystalline steps of the HOPG surface into 1D lines. The STM topography image of an isolated molecule of (**1**) appears as a bright uniform spot with a cross-section of about 1.7 nm surrounded by a less defined halo (Fig. 3c). The halo can be attributed to contributions of the BF_4^- anions and solvent molecules. The overall size of the spot fits well to the molecular size extracted from single crystal X-ray diffraction studies (1.65 nm in the square).[22] Besides some faint features, room temperature STM topography of (**1**) does not provide any further information concerning the submolecular structure.

To gain further information, CITS was applied to the (**1**)–HOPG system. In order to avoid redox processes, the investigations were confined to negative sample-to-tip bias voltages, *i.e.* to the tunneling spectroscopy of occupied molecular energy levels. The CITS current map of assembly (**1**) exhibits a square array of four bright spots representing sharp local peaks in the tunneling current (Fig. 3d). The distance between the emerging maxima is approximately 0.7 nm, which corresponds to the Co–Co distance between two neighboring metal ions obtained by single crystal X-ray diffraction investigations.[22] Under the experimental conditions, no additional features arising from the four bis(bipyridyl)pyrimidine ligands $\mathbf{L^1}$ were observed.

In Fig. 4, a 3D representation of the DFT electron density maps using the same colouring scheme as for the experimental data (bottom) is shown for two different energy windows: The first one covers the range between E_F and the HOMO (−0.55 eV), while the second one covers the full range between E_F and −1.0 V, where all states exhibiting 3d-character are expected to be found. As already discussed in Section 2, the LUMO is expected to be pinned close to E_F due to the high positive charge (eight-fold) of (**1**). Considering that DFT usually underestimates band gaps, the HOMO–LUMO gap seems to be by 150 meV too small in comparison with the tunneling experiment. As a consequence, the theoretical distribution at −0.55 eV should so conform to the map of tunneling currents at a bias of −0.7 V. The experimental data given in Fig. 4 (bottom) exhibit the central part of the CITS map with subtracted background proving the agreement between experimental and theoretical data.

By measuring the set of *I–V* characteristics along a straight line between the two arrows in Fig. 3b, a drastic increase of the tunneling current beyond a threshold voltage of approximately −0.6 V is observed at the presumed positions of the metal ion cornerstones (Fig. 5 right). This can be explained by the sudden accessibility of the HOMO of (**1**), which has strong Co 3d character, for the tunneling current (Fig. 5 left). The DFT calculated DOS (density of states) curves in Fig. 5 were obtained from a spin-polarized calculation with antiferromagnetic ordering of the Co ions. The two spin directions are shaded in black and red. The further increase of the experimental *I–V* characteristics around −1 V conforms to the second peak in the calculated DOS curve of the Co 3d states. We emphasize that the influence of the N 2p states is negligibly small (Fig. 5, lower panel). Furthermore, any other ligand states such as C 2s, 2p, or N 2s do not contribute to the energy interval of ± 1 eV around the Fermi level. Thus DFT calculations confirm that all peak features in the experimental CITS maps are exclusively caused by the Co^{II} ions.

In the same line, CITS investigations were carried out on the [3 × 3] Mn^{II}_9 assembly $[Mn^{II}_9(\mathbf{L^2})_6](ClO_4)_6$ (**2**), a higher homologue of the above described [*n* × *n*] grid-like class (Fig. 6a and b). The spatially resolved CITS map of an isolated

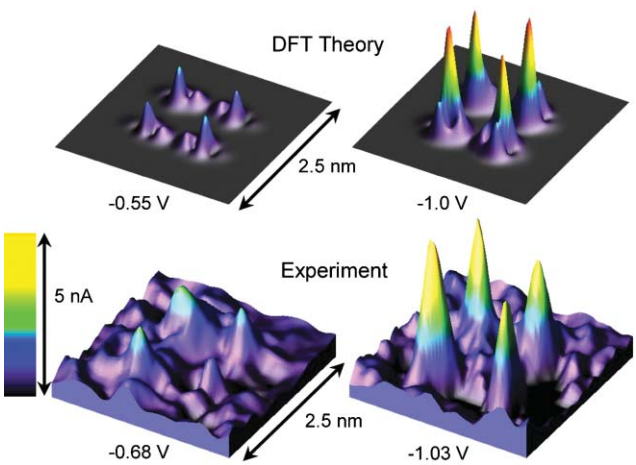

Fig. 4 (Top) 3D representation of DFT calculated electron density maps within an energy window between E_F and $E = -0.55$ eV (left) and between E_F and $E = -1.0$ eV (right); (bottom) central section of the measured CITS maps at −0.68 V and −1.03 V.

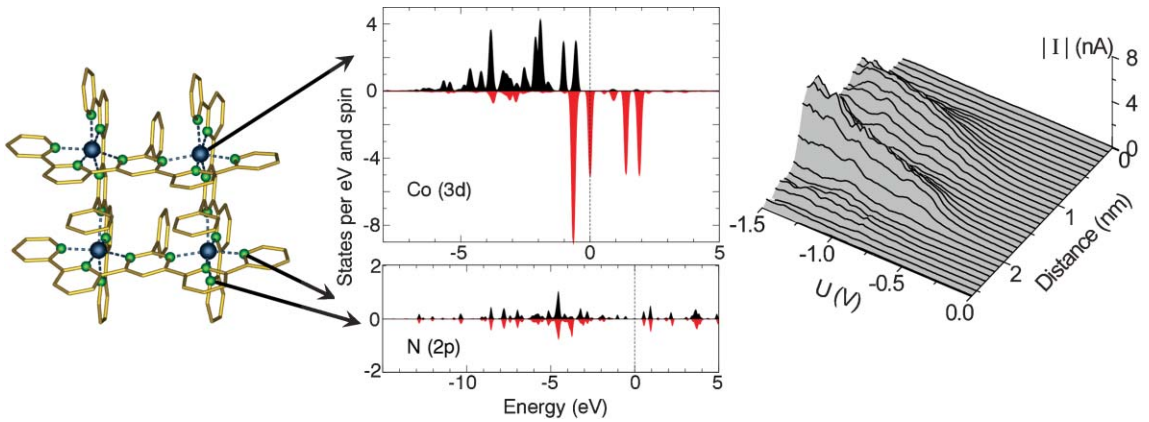

Fig. 5 Left) X-ray crystal structure of (**1**) with the local density of states (DOS) for a Co ion and for a coordinating N donor atom calculated by DFT. For better comparison both DOS curves have the same vertical scale; right) representation of a set of *I–V* characteristics measured along the line between two Co^{II}-ion cornerstones as marked by arrows in Fig. 3d. The background current arising from tunnelling into the substrate has been subtracted.

[3 × 3] grid-like assembly, taken at a bias of −0.73 V below the Fermi-level, reveals a regular array of nine tetragonally aligned sharp maxima at shorter distances than found for (**1**) (Fig. 6d). These shorter peak-to-peak distances of around 0.4 nm correspond exactly to the Mn–Mn distances within (**2**) obtained from the single crystal X-ray structure.[23] The puckered environment of the tunneling current maxima marks the molecular dimensions (molecular footprint of 2.4 × 2.4 nm). The peaks reflect the structural features of the [3 × 3] Mn^{II}_9 grid-like complex exhibiting the regular arrangement of the metal ions (Fig. 6d). Once more, no features of the interconnecting ligands $\mathbf{L^2}$ could be detected by CITS.

4. Star-like supramolecular metal ion assemblies

Since the discovery of the first single-molecule magnet (SMM) Mn_{12}-acetate in the early nineties, a variety of molecules with similar magnetic properties have been investigated by various experimental and theoretical techniques. In SMMs the intramolecular magnetic coupling of paramagnetic ions leads to a high-spin ground state. An anisotropy of the easy-axis type is crucial, as it creates the required energy barrier between the $M = -S$ and the $M = +S$ groundstates leading to the long relaxation time of the strongly anisotropic magnetic moment and quantum tunneling phenomena.[24]

A further entry of molecular compounds exhibiting such magnetic properties is the class of star-like supramolecular metal ion assemblies. The molecular structure of star-like assemblies is characterized by a centered-trigonal topology of four Fe ions (Fig. 7b). In detail, the internal metal ion arrangement within star-like supramolecular assemblies is such that the three peripheral Fe ions are oxo-bridged to the single central one. As there is no magnetic coupling path going along the periphery, no ferromagnetic interaction is required for establishing a high-spin groundstate. In the case of four Fe(III) metal ions, a $S = 10/2$ groundstate is generated by only the topological arrangement with antiferromagnetic coupling between the metal ions. Together with an easy-axis type of magnetic anisotropy and a rather large gap to the first exited state, trigonal metal-centered $\{FeFe_3\}$ supramolecular assemblies as $\{Fe^{III}[Fe^{III}(\mathbf{L^3})_2]_3\}$ (**3**) are among the simplest inorganic systems showing single-molecule magnet behaviour (Fig. 7a and b).[25,26]

The metal ion assembly (**3**) was synthesized from ligand *N*-methyldiethanolamine $H_2\mathbf{L^3}$ and ferric chloride in the presence of sodium hydride. Magnetically, (**3**) shows a blocking temperature of approximately 1.2 K. The ligand-field splitting parameters have been determined by EPR measurements with $D = -0.57$ K, $E = 56$ mK, $B^{04} = -30$ μK, $B^{24} = -390$ μK, $B^{44} = 60$ μK.[27]

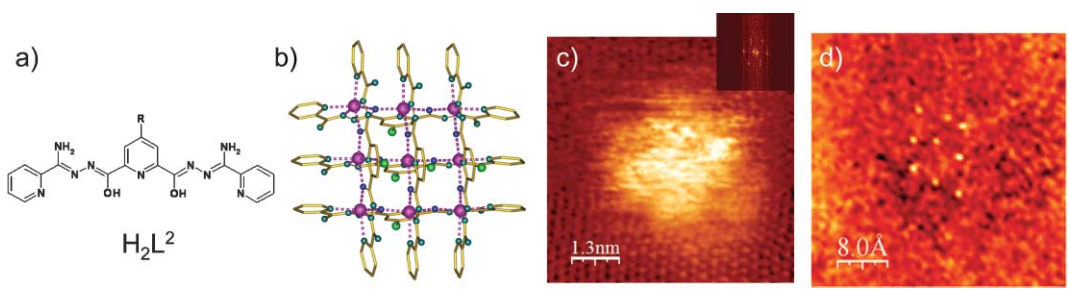

Fig. 6 [3 × 3] grid-like complexes: Molecular structure of a) the ligand $H_2\mathbf{L^2}$ and b) the X-ray structure of the grid-like $[Mn^{II}_9(\mathbf{L^2})_6](ClO_4)_6$ (**2**); c) topographic STM image; the inset shows a 2D Fourier transform with the hexagonal pattern arising from the HOPG substrate and d) an experimental CITS map at −0.73 V.

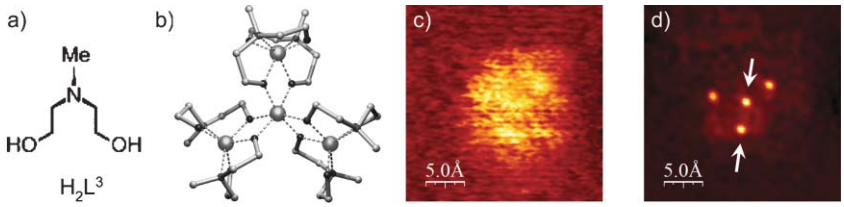

Fig. 7 Star-like metal ion assemblies: Molecular structure of a) ligand $H_2\mathbf{L}^3$ and b) representation of the X-ray structure of the star-like complex $\{Fe^{III}[Fe^{III}(\mathbf{L}^3)_2]_3\}$ (**3**); c) topographic STM image and d) image of the experimental CITS map at −0.918 V.

By extrapolating from the CITS results of the grid-like complexes, it can be expected that also in the case of (**3**) the level structure around E_F will be dominated by the Fe 3d states. Therefore, it can be assumed that CITS images would reveal a map of the Fe ions exclusively. This is of particular interest because then the magnetic signature of a single spin center could be investigated using methods like spin-polarized tunneling. CITS on HPOG substrate was used to determine the internal structural and electronic properties of isolated assemblies of (**3**).

Topographic STM investigations have proven the star-like shape of the molecule with a diameter of approximately 1.3 nm, which conforms to the outer diameter of the molecule (Fig. 7c). The submolecular electronic properties of the star-like complex (**3**) were investigated by CITS as depicted in Fig. 7d. The CITS map at a bias voltage of −0.918 V shows four bright maxima of the tunneling current which form a star-like pattern. Some smaller satellites were also observed. The distances between the bright tunneling current maxima correspond to the distance between the central and the peripheral Fe ions within the assembly (0.32 nm).[26] As all distances between the peaks conform to the Fe–Fe distances in the complex, it was concluded that the local maxima of the density of states correspond to the positions of the Fe ions of (**3**).

The following conclusions can de drawn from the DFT calculation of the charge density at different energies: As the bias voltage becomes more negative starting from zero, the peripheral Fe atoms yield the first signal, followed by the central Fe atom at lower voltages. Simultaneously, much weaker features due to the apical oxygens appear as wings next to the Fe peaks (Fig. 8a and b). This behavior was also observed in the CITS maps as a function of bias voltage. Fig. 8a and b represent the spatial distribution of the electron density due to the states situated within an energy window of 0.95 eV downwards from the Fermi energy. The comparison with the experimental CITS maps of (**3**) (Fig. 8c) provides satisfactory agreement between theory and experiment.

The spin-resolved DFT calculations of the local density of states of (**3**) (Fig. 9a) show that the region around the Fermi energy E_F hosts Fe 3d states, which are strongly spin split and strongly hybridized with the O 2p states. The two spin directions are discriminated by black and red shading. There is a "band gap" of ≈0.95 eV between the highest occupied and the lowest unoccupied molecular orbitals, both being of mostly Fe 3d–O 2p character. The states with energies below −6 eV are all a mixture of different orbitals forming covalent bonds and involving C 2s,2p, N 2s,2p states, and O 2s and 2p levels.[27] As the most important result of the DFT calculations it can be stated that the DOS landscape around the Fermi energy is dominated by Fe 3d states. There are only weak contributions from the apical and bridging oxygens; the rest of the molecule is completely transparent within the energy interval of ± 1 eV around the Fermi level (Fig. 9a).

In addition, the spatially resolved *I–V* characteristics, taken along the line between the two arrows in Fig. 7d, reveal that the central Fe ion can be discrimated spectroscopically from the peripheral ones by its different DOS character. Thus, the experimental CITS map reveals kinks in the *I–V* characteristics centered at −0.57, −0.74, −0.92 V for the central ion and −0.36, −0.70, −0.87 V for the peripheral ion (Fig. 9 right). This is in excellent agreement with the DFT DOS peaks at −0.55, −0.72, −0.91 eV for the central ion and −0.33, −0.67, −0.83 eV for the peripheral ion (Fig. 9 left).

5. Infinitely extended metal ion assemblies: Coordination polymers

1D coordination polymer assemblies have attracted much attention in the development of new functional materials owing to such properties as zeolitic behavior, conductivity, luminescence, magnetism, spin-crossover, and nonlinear

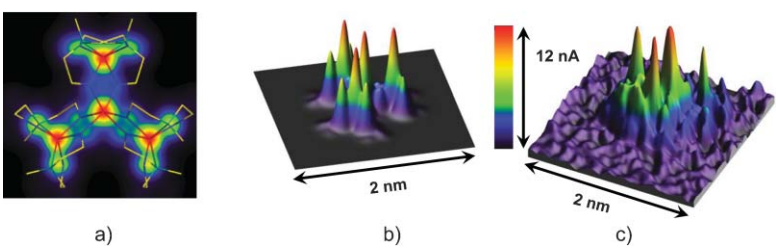

Fig. 8 (a) Colour coded map of the DFT calculated charge density of (**3**) within an energy window between E_F and −0.95 eV in superposition with the crystal structure data (sticks), the scale is 1.2 × 1.2 nm; b) 3D representation of the DFT electron density map; (c) 3D representation of the central section of the experimental CITS map taken at −0.918 V.

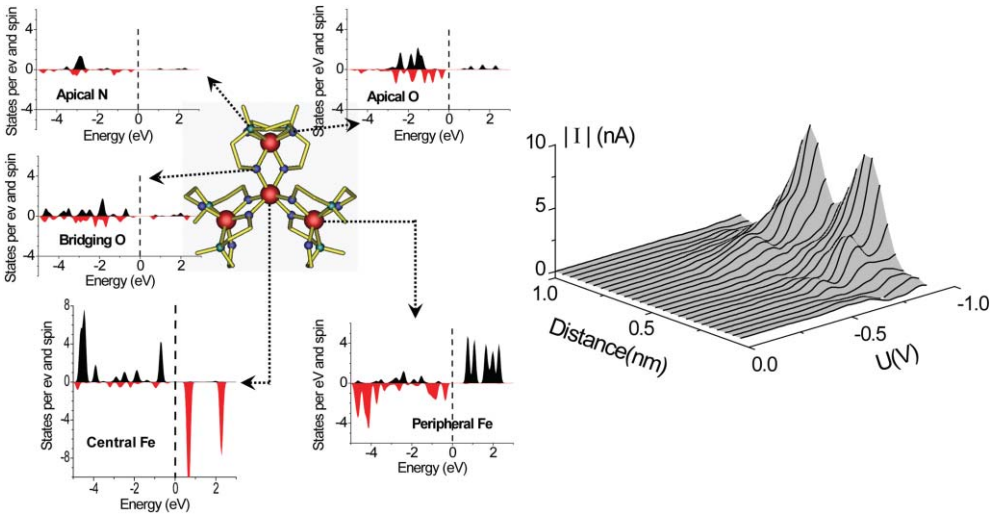

Fig. 9 left) X-ray crystal structure of (**3**) plotted together with local densities of states (DOS) of all atoms participating in the coordination of the Fe ions. For better comparison, all DOS curves are represented in the same scale; right) set of *I–V* characteristics along the line from the central to one peripheral Fe^{III}-ion (arrows in Fig. 7d).

optical effects.[28] Yet the equally important controlled assembly of metal–organic polymers on solid surfaces is in its infancy. A central focus of this research is the investigation of elementary structure–formation processes on substrate surfaces.[7] A series of structurally similar polymers containing different aromatic amino acid building blocks was investigated in order to estimate the influence of the substituents on the local surface properties. Towards this end, the cationic coordination polymer $\{[Zn(\mathbf{L^4})]_n\}(CF_3\ SO_3)_n$ (**4**) ($\mathbf{L^4}$ = dipicolylglycyl tyrosine) was deposited on highly ordered pyrolytic graphite (HOPG) and investigated with regard to its local tunneling properties (Fig. 10a).[29]

Samples of (**4**) on HOPG were conveniently prepared by allowing 10^{-9} M aqueous solutions of pH 5 to 6 to evaporate in air. It was shown by topographic STM investigations that the polymer adopts two different structures depending on the local environment of the substrate: (i) a double-helical plait is formed on undisturbed flat surface areas and (ii) linearly stretched polymer strands are formed along the steps of the substrate (see Fig. 10b).[29] Apparently, the structure change is a consequence of differing strength polymer–substrate interactions between (**4**) and the HPOG. To further prove the structure of the linearly stretched polymer strand, CITS investigations were carried out. A current image taken at a tunneling bias of −0.135 V is shown in Fig. 10c. Whereas the signature of single Zn(II) metal centers is not visible, one clearly recognizes an intensity modulation on a scale of 1.5 nm conforming to the length of one monomer (white bar in Fig. 10c).

6. Polyoxoanions

Polyoxometallates (POMs) are early-transition-metal oxygen clusters with a great variety of shape, size, and composition.[30] This class of compounds, often described as soluble metal-oxide fragments, has received increasing attention recently, mostly due to its multitude of interesting catalytic, electronic, magnetic, medical, thermal, and optical properties.[31] Recently, the synthesis of an unprecedented Cu_{20}-containing polyoxotungstate of large size and high symmetry by self-assembly techniques was reported.[32] The wheel-shaped $[Cu_{20}Cl(OH)_{24}(H_2O)_{12}(P_8W_{48}O_{184})]^{25-}$ (**5**) represents the first transition metal-substituted derivative of $[H_7P_8W_{48}O_{184}]^{33-}$ and incorporates more Cu^{2+} ions than any other polyoxometalate known to date (Fig. 11a and b).[31] The electrochemical properties of (**5**) have also been reported.[33]

Certainly, POM's are interesting on their own; however, their ability to form large and open cage-like arrays may also

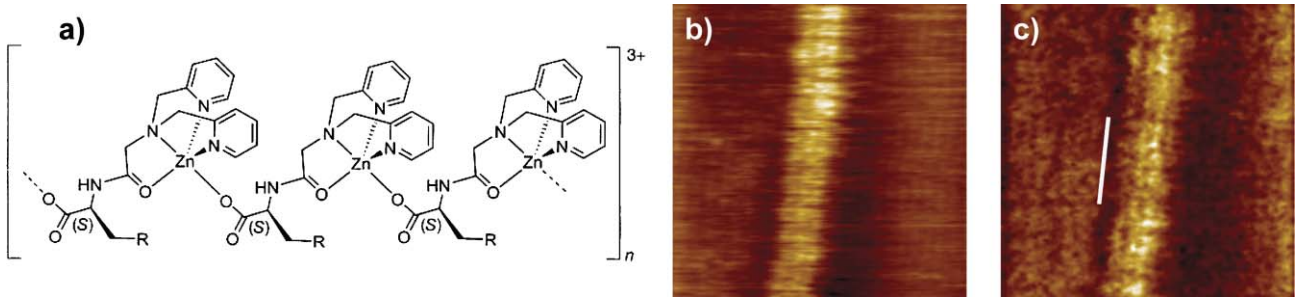

Fig. 10 The cationic coordination polymer $\{[Zn(\mathbf{L^4})]_n\}(CF_3\ SO_3)_n$ (**4**): a) representation of the molecular structure, R = Ph-OH; b) topographic STM image; c) experimental CITS map at −0.135 V. The white bar shows the length of one monomer.

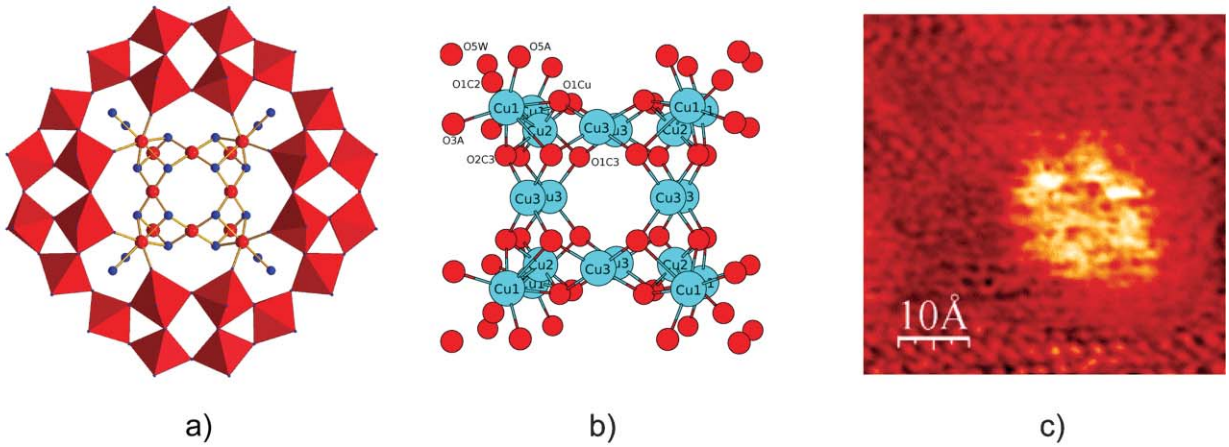

Fig. 11 The polyoxometallate anion $[Cu_{20}Cl(OH)_{24}(H_2O)_{12}(P_8W_{48}O_{184})]^{25-}$ (**5**): a) schematic representation of the molecular structure; b) perspective view of the central Cu_{20} cluster; c) topographic STM image.

provide containers for other types of materials. The present Cu_{20} wheel can be considered as an oxygen–copper cage sitting as a hub in the center of a large polyoxotungstate wheel. The Cu_{20} cluster is therefore effectively shielded from the environment but sufficiently open for investigations with the STM. The topographic image in Fig. 11c depicts only a rough shape of the overall structure of the molecule. However, the CITS image shown in Fig. 12a, taken at a bias voltage of −0.913 V, exhibits a square array of eight bright spots which represent sharp peaks of the tunneling current. This can be seen even more clearly in the perspective 3D representation of the CITS map in Fig. 12b. These peaks can be associated with the position of the Cu atoms gained from X-ray investigations as shown in Fig. 11a and b. As in this projection the Cu1 and Cu2 atoms in the corners are rather close to each other, they are mapped in the CITS image only as one single spot. The average distance between neighboring peaks is 0.28 nm, conforming well to the distance of 0.27 nm between the average position of the projection of Cu1 and Cu2 and the Cu3 position, as obtained from X-ray diffraction.[34] Noteworthy, there is a steep current increase at voltages below −0.4 V. Despite the high resolution of the current images, no remarkable features arising from the μ_3-oxo ligands were detectable. Obviously, the local maxima of the DOS at the position (of the projection on the plane) of the Cu atoms have been mapped. Therefore, it is rather interesting to compare these experimental results with the electronic structure of the complex.

Due to its structural complexity and its high negative charge, the theoretical interpretation of the CITS results of the polyanion (**5**) is not straightforward. The DFT calculations show that the occupied states situated within an energy window of 0.9 eV below the chemical potential have a substantial contribution from the 3d states of the Cu1–Cu2–Cu1 trimers, but only a rather small one from the cube-edge Cu3 atoms. Moreover, the 2p states of the oxygen atoms within the PO_4 groups and the water molecules close to the Cu trimers provide an essential contribution within this energy window (Fig. 13). This is quite different from what is seen in the experimental CITS images (Figs. 12a and b), where the contribution from all Cu atoms is present with similar intensity and no intensity can be seen at the positions of the oxygen atoms. However, within 0.9 eV above the chemical potential, the unoccupied states are of about equal intensity for all Cu atoms, and exclusively for them, *i.e.*, there is no contribution from any of the oxygen sites. Fig. 12c shows the electron density of unoccupied states, integrated over an energy interval of 0.9 eV above the chemical potential. The similarity to the measured STS data at a bias of −0.913 V (Fig. 12b) is striking.

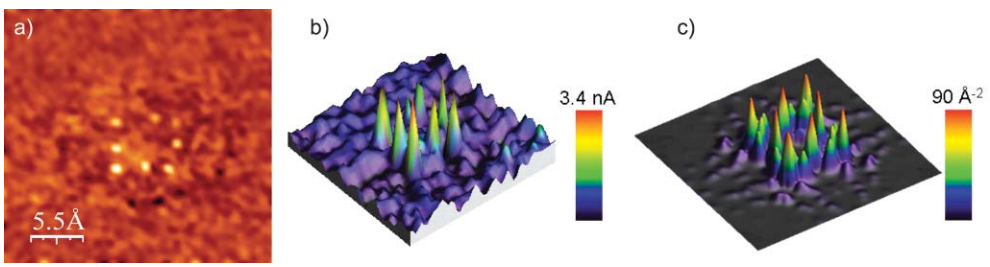

Fig. 12 The polyoxometallate anion $[Cu_{20}Cl(OH)_{24}(H_2O)_{12}(P_8W_{48}O_{184})]^{25-}$ (**5**): a) experimental CITS current map at −0.913 V showing the projection of the Cu^{II} metal ions as eight bright spots; b) 3D view in a different color palette; c) 3D representation of the calculated electron density, integrated over an energy interval of 0.9 eV above the chemical potential and along the *z* axis throughout the molecule.

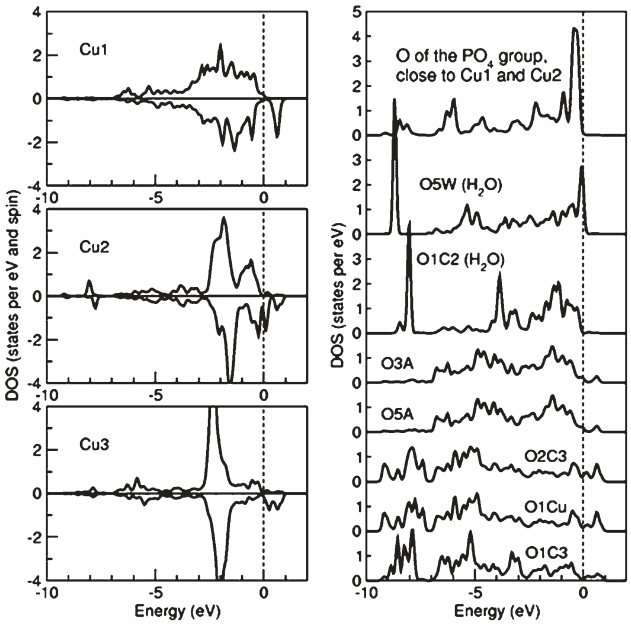

Fig. 13 Local DOS at three different Cu sites (left panel) and at eight different O sites (right panel) of the Cu_{-20} polyanion obtained from the DFT calculation. The labeling is explained in Fig. 5b. The dashed line at 0 eV separates occupied and vacant states. The continuous DOS was obtained from broadening the discrete energy levels of the isolated molecular fragment with a width parameter of 0.1 eV.

As the substrate potential was always negative with respect to the tip, one would expect only probing of the occupied levels because electrons are extracted from the molecule. However, as soon as there is a substantial energy barrier between substrate and molecule, the potential of the molecule is "sweeping" between those of substrate and tip. The exact alignment of the molecular levels relative to the chemical potentials of substrate or tip depends sensitively on the heights of the barriers between substrate and molecule and between molecule and tip. In fact, it is influenced rather delicately by the charge balance between molecule and substrate, as well as by the distance between the tip and the molecule. It is easy to recognize that tunneling *via* the unoccupied levels is possible even if the electron transport goes from the substrate *via* the molecule into the tip. By varying the initial voltage and current settings, the tip-to-molecule distance could be varied such that maximum contrast in the CITS images was obtained. An inspection of the DFT results shows that the maximum contrast between Cu-related (*i.e.*, the eight-dot array seen in Fig. 12a and b) and not-Cu-related contributions might be achieved if one probes the lowest unoccupied levels, which are the vacant Cu d states. The adequacy of our interpretation of CITS images through the involvement of unoccupied states can be clearly seen by a comparison of Fig. 12b and c.

7. Metal ion coordination in supramolecular assemblies

The self-assembly of well defined metallo-supramolecular architectures mostly involves organic ligands and metal ions. The ligands arrange the metal ion into special topologies, which are determined by the design of the ligands (kind of donor atoms and their spatial arrangement, steric crowding, *etc.*) and the electronic character of the metal ions (involved s-, p-, d- or f-orbitals, redox and spin states, ionization energies, *etc.*), which altogether determines a certain coordination algorithm. In this way, the concerted interaction between metal ions and ligands chooses from a predetermined set of coordination geometries, as found *e.g.* in the distorted octahedral for Co(II)-, Mn(II)-, and Fe(III)-metal ions in compounds (**1**), (**2**), and (**3**) or trigonal-bipyramidal for the Zn(II) metal ions in compound (**4**). Moreover, several coordination geometries can be expressed for one type of metal ion within the same architecture, as seen for the Cu(II) metal ions in compound (**5**) displaying Jahn–Teller-distorted octahedral and, additionally, two different kinds of square pyramidal coordination geometries.

Since CITS has to be understood as the spatially resolved mapping of the electron density of the molecular orbitals, involved in the tunneling process during the experiment, a view on the molecular orbital scheme for the case of d-metals (all herein involved metal ions are d-metals) in an octahedral ligand field (most of the entities treated here involve octahedral metal coordination) may be very helpful. Fig. 14 shows the schematic molecular orbital diagram for a Co(II) metal ion interaction with σ-donating ligands in O_h symmetry (a situation very similar to that found for the cornerstone metal ions in compound (**1**)).[35] As can be seen, the σ-donated ligand electrons occupy the six lowest bonding orbitals. The remaining electrons, originating from the d^7 configuration of the

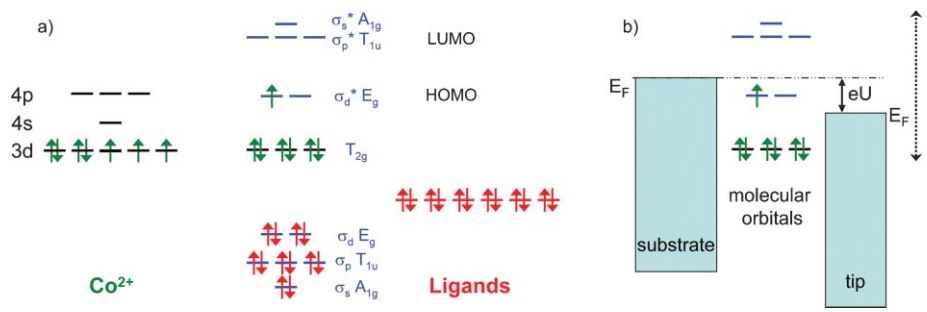

Fig. 14 a) Schematic molecular orbital diagram for the σ bonding of a Co^{2+} ion (left) implying six ligands in an octahedral environment around the metal ion; b) simplified picture of the tunneling process: as soon as a molecular level becomes resonant with the Fermi energy E_F of either the substrate or the microscope's tip, the tunneling current is rising. The maximum range of bias voltage is sketched by the arrow on the right hand side.

Co(II) metal ion, are placed into the non-bonding t_{2g} orbitals and into the antibonding e_g* orbitals, whereby it is presumed that the final configuration of the metal ion is low spin. The lowest six filled orbitals provide an account of the binding, attractive forces between the metal ion and the pyridine-type ligands. Above them, either the non-bonding t_{2g} orbitals or the antibonding e_g* orbitals constitute the HOMO of the molecule, depending upon the number of electrons distributed there following the d^n configuration of the involved metal ion.

By putting the molecule into the electrical field established between tip and substrate, as done during tunneling spectroscopy, it becomes possible to map the respective HOMO's or LUMO's of the molecule within an energy range of approximately ± 1.5 eV depending on the sign of the applied potential U (Fig. 14b). An experimental difficulty is, however, the a priori unknown shift of the molecule's Fermi level relative to the potential of the substrate, as a tunneling barrier between substrate and molecule cannot be ruled out. By changing the tunneling bias U, it is possible to filter out locally all molecular orbitals, which are involved in the metal ion binding. All other molecular orbitals, *e.g.* those constituting the covalent bonds of the organic ligands, will be only mapped at much higher energies. In this sense, it becomes possible to screen exclusively for the location of the coordination bonds within the supramolecular assemblies rendering the positions of the metal ions with submolecular spatial resolution.

8. Conclusions

In conclusion, several supramolecular metal ion assemblies of different structural complexity and incorporating different transition metal ions were deposited on HOPG and investigated by scanning tunneling microscopy (STM) and current imaging tunneling spectroscopy (CITS). The molecules were drop-cast from their solution onto the HOPG substrate and investigated under ambient conditions at room temperature. Topographically, the observed spatial dimensions of the single molecules found on the surface were in accordance with the data determined by X-ray crystallography. CITS investigations allowed the localization of the positions of the incorporated transition metal centers due to a selective mapping of the coordinative metal–ligand bonds. This experimental approach is supported by ligand field considerations involving only the highest occupied molecular orbitals (HOMOs), which possess strong coordinative bond character, in the tunneling process. The experimentally determined local positions of the metal ions were confirmed by first principle density functional theory calculations.

CITS investigations involving straightforward sample preparation by drop casting and measurements under ambient conditions represent a general STM approach to address the metal centers within supramolecular assemblies with submolecular spatial resolution. An essential prerequisite is a low-drift microscope. It has to be mentioned that ultra high vacuum (UHV) STM techniques are capable of providing at least a similar resolution, however, the introduction of large supramolecular entities into the UHV chamber set up still constitutes a significant difficulty. In this sense, CITS at ambient conditions is a practicable and straightforward alternative to address metal centers within supramolecular metal ion assemblies by spectroscopic tunneling techniques, even if these ions are buried by the constituting organic ligand material. In view of the great diversity of possible transition metal centers incorporated into supramolecular architectures and their very broad variation of genuine redox-, electronic and spin state properties, CITS might become an indispensable tool for addressing active metal ions at the single "ion dot" level. Towards this end, work is in progress to extend the applicability of CITS to other types of metal ions (*e.g.* s- or f-metals), as well as to enable the direct spectroscopic monitoring of metal ion properties such as redox or spin states.

References

1 ENIAC-Strategic Research Agenda, *European Technology Platform Nanoelectronics*, November, 2005, under http://www.cordis.lu/ist/eniac.

2 J.-M. Lehn, *Supramolecular Chemistry. Concepts and Perspectives*, VHC, Weinheim, 1995; J.-M. Lehn, *Science*, 2002, **295**, 2400–2403; J.-M. Lehn, *Proc. Natl. Acad. Sci. U. S. A.*, 2002, **99**, 4763–4768.

3 M. Ruben, J. Rojo, F. J. Romero-Salguero, L. H. Uppadine and J.-M. Lehn, *Angew. Chem., Int. Ed.*, 2004, **43**, 3644–3662 and references therein.

4 J. Park, A. N. Pasupathy, J. I. Goldsmith, C. Chang, Y. Yaish, J. R. Petta, M. Rinkowski, J. P. Sethna, H. D. Abruna, P. L. McEuen and D. C. Ralph, *Nature*, 2002, **417**, 722–725.

5 M. Ruben, *Angew. Chem., Int. Ed.*, 2005, **44**, 1594–1596; N. Lin, S. Stepanow, F. Vidal, K. Kern, M. S. Alam, S. Strömsdöfer, V. Dremov, P. Müller and M. Ruben, *Dalton Trans.*, 2006, 2794–2800.

6 S. De Feyter and F. C. De Schryver, *Chem. Soc. Rev.*, 2003, **32**, 139; P. Samorí, *Chem. Soc. Rev.*, 2005, **34**, 551–561.

7 (*a*) A. Miura, Z. Chen, H. Uji-i, S. De Feyter, M. Sdanowska, P. Jonkhejm, A. P. H. J. Schenning, B. Mejer, F. Würthner and F. C. De Schryver, *J. Am. Soc. Chem.*, 2003, **125**, 14968–14969; (*b*) A. Gesquiere, S. De Feyter and F.C. De Schryver, *Nano Lett.*, 2001, **1**, 201–206; (*c*) F. Jäckel, M. D. Watson, K. Müllen and J. P. Rabe, *Phys. Rev. Lett.*, 2004, **92**, 188303.

8 (*a*) Ó. Paz, I. Brihuega, J. M. Gómez-Rodríguez and J. M. Soler, *Phys. Rev. Lett.*, 2005, **94**, 056103; (*b*) S. D. Feyter and F. C. D. Schryver, *J. Phys. Chem. B*, 2005, **109**, 4290; (*c*) S. Hembacher, F. J. Giessibl and J. Mannhart, *Phys. Rev. Lett.*, 2005, **94**, 056101.

9 *Scanning Tunneling Microscopy*, ed. J. A. Stroscio and W. J. Kaiser, Academic Press, New York, 1993.

10 R. J. Hamers, R. M. Tromp and J. E. Demuth, *Phys. Rev. Lett.*, 1986, **56**, 1974.

11 M. Rivera, R. L. Williamson and M. J. Miles, *J. Vac. Sci. Technol., B*, 1996, **14**, 1472.

12 M. S. Alam, PhD Thesis, Universität Erlangen-Nürnberg, 2006.

13 D. V. Porezag and M. R. Pederson, *Phys. Rev. A*, 1999, **60**, 2840; M. R. Pederson, D. V. Porezag, J. Kortus and D. C. Patton, *Phys. Status Solidi B*, 2000, **217**, 197.

14 http://www.uam.es/siesta; (*a*) P. Ordejón, E. Artacho and J. M. Soler, *Phys. Rev. B*, 1996, R10441; (*b*) J. M. Soler, E. Artacho, J. D. Gale, A. García, J. Junquera, P. Ordejón and D. Sánchez-Portal, *J. Phys.: Condens. Matter*, 2002, **14**, 2745.

15 A. Postnikov, J. Kortus and M. R. Pederson, *Phys. Status Solidi B*, 2006, **243**, 2533.

16 M. Ruben, E. Breuning, J.-P. Gisselbrecht and J.-M. Lehn, *Angew. Chem., Int. Ed.*, 2000, **39**, 4139–4142; M. Ruben, E. Breuning, M. Barboiu, J.-P. Gisselbrecht and J.-M. Lehn, *Chem.–Eur. J.*, 2003, **9**, 291–299; D. M. Bassani, J.-M. Lehn, S. Serroni, F. Puntoriero and S. Campagna, *Chem.–Eur. J.*, 2003, **9**, 5936–5946.

17 O. Waldmann, J. Hassmann, P. Müller, G. S. Hanan, D. Volkmer, U. S. Schubert and J.-M. Lehn, *Phys. Rev. Lett.*, 1997, **78**, 3390.

18 E. Breuning, M. Ruben, J.-M. Lehn, F. Renz, Y. Garcia, V. Ksenofontov, P. Gütlich, E. Wegelius and K. Rissanen, *Angew. Chem., Int. Ed.*, 2000, **39**, 2504–2507; M. Ruben,

E. Breuning, J.-M. Lehn, V. Ksenofontov, F. Renz, P. Gütlich and G. Vaughan, *Chem.–Eur. J.*, 2003, **9**, 4422–4429; M. Ruben, U. Ziener, J.-M. Lehn, V. Ksenofontov, P. Gütlich and G. B. M. Vaughan, *Chem.–Eur. J.*, 2005, **11**, 94–100.
19 A. Semenov, J. P. Spatz, M. Möller, J.-M. Lehn, B. Sell, D. Schubert, C. H. Weidl and U. S. Schubert, *Angew. Chem., Int. Ed.*, 1999, **38**, 2547.
20 M. Ruben, J.-M. Lehn and G. Vaughan, *Chem. Commun.*, 2003, 1338–1339.
21 M. S. Alam, S. Strömsdörfer, S. Dremov, P. Müller, J. Kortus, M. Ruben and J.-M. Lehn, *Angew. Chem., Int. Ed.*, 2005, **44**, 7896–7899.
22 J. Rojo, F. J. Romero-Salguero, J.-M. Lehn, G. Baum and D. Fenske, *Eur. J. Inorg. Chem.*, 1999, 1421.
23 V. A. Milway, S. M. Tareque Abedin, V. Niel, T. L. Kelly, L. N. Dawe, S. K. Dey, D. W. Thompson, D. O. Miller, M. S. Alam, P. Müller and L. K. Thompson, *Dalton Trans.*, 2006, 2835.
24 R. Sessoli, D. Gatteschi, A. Caneschi and M. A. Novak, *Nature*, 1993, **365**, 141.
25 A. L. Barra, A. Caneschi, A. Cornia, F. Fabrizi de Biani, D. Gatteschi, C. Sangregorio, R. Sessoli and L. Sorace, *J. Am. Chem. Soc.*, 1999, **121**, 5302; A. Cornia, A. C. Fabretti, P. Garrisi, C. Mortal, D. Bonacchi, D. Gatteschi, R. Sessoli, L. Sorace, W. Wernsdorfer and A.-L. Barra, *Angew. Chem., Int. Ed.*, 2004, **43**, 1136.
26 R. W. Saalfrank, A. Scheurer, I. Bernt, F. W. Heinemann, A. V. Postnikov, V. Schünemann, A. X. Trautwein, M. S. Alam, H. Rupp and P. Müller, *Dalton Trans.*, 2006, 2865.
27 A. F. Takács, M. Neumann, A. V. Postnikov, K. Kuepper, A. Scheurer, S. Sperner, R. W. Saalfrank and K. C. Prince, *J. Chem. Phys.*, 2006, **124**, 044503.
28 C. Janiak, *Dalton Trans.*, 2003, 2781.
29 S. Novokmet, M. S. Alam, V. Dremov, F. W. Heinemann, P. Müller and R. Alsfasser, *Angew. Chem., Int. Ed.*, 2005, **44**, 803–806.
30 *Polyoxometalate Molecular Science*, ed. J. J. Borras-Almenar, E. Coronado, A. Müller and M. T. Pope, Kluwer, Dordrecht, The Netherlands, 2004.
31 *Polyoxometalate Chemistry: From Topology via Self-Assembly to Applications*, ed. M. T. Pope and A. Müller, Kluwer, Dordrecht, The Netherlands, 2001.
32 S. S. Mal and U. Kortz, *Angew. Chem., Int. Ed.*, 2005, **44**, 3777–3780.
33 D. Jabbour, B. Keita, L. Nadjo, U. Kortz and S. S. Mal, *Electrochem. Commun.*, 2005, **7**, 841.
34 M. S. Alam, V. Dremov, P. Müller, A. Postnikov, S. B. Mal, F. Hussain and U. Korz, *Inorg. Chem.*, 2006, 2866–2872.
35 M. Gerloch and E. C. Constable, *Transition Metal Chemistry*, VCH, Weinheim, Germany, 1994.